Resistance to action potential depression of a rat axon terminal in vivo

Martijn C. Sierksma[a] and J. Gerard G. Borst[a,1]

[a]Department of Neuroscience, Erasmus MC, University Medical Center Rotterdam, 3015 GE Rotterdam, The Netherlands

Edited by Bruce P. Bean, Harvard Medical School, Boston, MA, and approved March 9, 2017 (received for review November 24, 2016)

The shape of the presynaptic action potential (AP) has a strong impact on neurotransmitter release. Because of the small size of most terminals in the central nervous system, little is known about the regulation of their AP shape during natural firing patterns in vivo. The calyx of Held is a giant axosomatic terminal in the auditory brainstem, whose biophysical properties have been well studied in slices. Here, we made whole-cell recordings from calyceal terminals in newborn rat pups. The calyx showed a characteristic burst firing pattern, which has previously been shown to originate from the cochlea. Surprisingly, even for frequencies over 200 Hz, the AP showed little or no depression. Current injections showed that the rate of rise of the AP depended strongly on its onset potential, and that the membrane potential after the AP (V_{after}) was close to the value at which no depression would occur during high-frequency activity. Immunolabeling revealed that $Na_v1.6$ is already present at the calyx shortly after its formation, which was in line with the fast recovery from AP depression that we observed in slice recordings. Our findings thus indicate that fast recovery from depression and an inter-AP membrane potential that minimizes changes on the next AP in vivo, together enable high timing precision of the calyx of Held already shortly after its formation.

afterpotential | AP modulation | sodium channel inactivation | MNTB | synapse development

Action potentials (APs) are followed by a period of decreased excitability called the refractory period. High-frequency firing thus requires special adaptations to minimize this refractory period and maintain AP stability. The changes in the AP waveform that occur at high firing frequencies are especially relevant in presynaptic terminals, where the shape of the AP critically controls calcium influx via voltage-dependent calcium channels, and thus transmitter release (1, 2). Following the AP, the membrane potential during the recovery period has a large influence on the speed of the recovery from inactivation of voltage-dependent sodium channels and deactivation of voltage-dependent potassium channels, which are two major determinants of the refractory period (2). In some terminals, the AP is followed by a depolarizing afterpotential (DAP) (3–9), whereas in others a hyperpolarizing afterpotential (HAP) has been observed (10–14). The sign of this afterpotential depends on the resting potential (6, 7, 15), suggesting that the membrane potential following the AP (V_{after}) might be more important than the sign of the afterpotential.

The calyx of Held is a glutamatergic axosomatic terminal whose biophysical properties have been well studied (16). Its many release sites enable it to act as an inverting relay synapse within the auditory brainstem that reliably drives its postsynaptic partner, a principal neuron in the medial nucleus of the trapezoid body (MNTB), even at firing frequencies >200 Hz (17). Shortly after its formation, around postnatal day 2 (P2) in rodents (18–20), it already fires in characteristic high-frequency bursts in vivo (21, 22). In slice studies, a large DAP has been observed (3), to which resurgent sodium currents (23) make a prominent contribution, and which may promote high-frequency firing (15). With the exception of cerebellar mossy fiber terminals (4, 8), studies on the biophysical properties of mammalian presynaptic terminals have been performed ex vivo, and the functional significance of afterpotentials, including their role during natural firing patterns, is currently largely unknown. Here, we make in vivo juxtacellular and whole-cell recordings from the calyx of Held in rat pups, and study how the afterpotentials contribute to the stability of presynaptic APs during natural firing patterns.

Results

Identification of in Vivo Calyces. To study the contribution of AP depression during physiological firing, we made blind juxtacellular and whole-cell recordings from the calyx of Held in 2- to 8-d-old rat pups. Several converging lines of evidence indicated that we indeed recorded from the calyx of Held, a giant terminal in the auditory brainstem. First, the identity of several calyces was confirmed by biocytin filling and subsequent histological processing (Fig. 1*A*; $n = 6$), revealing the typical cup shape of the calyx (Movie S1) and an axon that could often be traced back to the midline and to other auditory nuclei ipsilateral of the MNTB. Second, in agreement with previous calyceal recordings in slices (3, 24), terminals responded to constant-current injections with a single, brief, and overshooting AP at the start of the current injection, strong outward rectification, and a hyperpolarization-activated, depolarizing voltage sag (Fig. 1*B* and Fig. S1). Third, in some recordings, the calyceal AP was followed by a small deflection that likely reflects the postsynaptic AP (arrow in Fig. 1*C*). Fourth, the terminals showed a characteristic firing pattern, consisting of minibursts with high firing frequencies (Fig. 1*D*) (22, 25, 26). Its interval distribution resembled auditory nerve activity at this age (Fig. S2), which is in agreement with its generation by the cochlea (25). In contrast to in vivo postsynaptic recordings (22), no fast synaptic transients were observed in voltage-clamp mode (Fig. 1*E*), which is consistent with the absence of axo-axonal inputs. Therefore, the structures that we recorded from are highly likely to be calyces.

Significance

During high-frequency firing, the shape of a presynaptic action potential (AP) can alter, thereby changing neurotransmitter release. In this paper, we describe how a giant terminal in the brainstem of newborn rats called the calyx of Held can fire in vivo at high frequencies without substantial AP depression. The underlying mechanism was found to be the presence of sodium channels that can recover rapidly from depression in combination with a close match between the potential that is attained following an AP with the potential that maximizes AP stability. Surprisingly, this match was already there shortly after formation of the calyx of Held. We speculate that these mechanisms help synapses to maximize timing precision during high-frequency firing.

Author contributions: M.C.S. and J.G.G.B. designed research; M.C.S. performed research; M.C.S. and J.G.G.B. analyzed data; and M.C.S. and J.G.G.B. wrote the paper.

The authors declare no conflict of interest.

This article is a PNAS Direct Submission.

[1]To whom correspondence should be addressed. Email: g.borst@erasmusmc.nl.

This article contains supporting information online at www.pnas.org/lookup/suppl/doi:10.1073/pnas.1619433114/-/DCSupplemental.

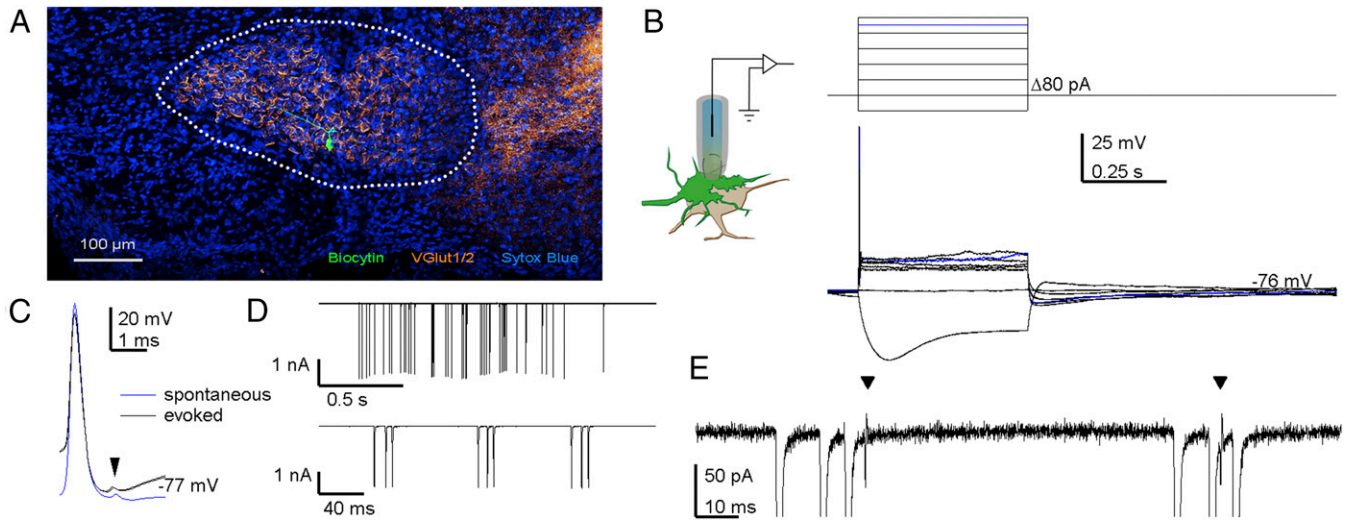

Fig. 1. Establishing in vivo recordings from the calyx of Held. (*A*) Coronal section of the P6 rat ventral brainstem containing the MNTB (outlined) labeled with anti-biocytin (green), anti-vesicular glutamate transporter 1 and 2 (orange), and the nucleotide stain Sytox Blue. The midline is located to the *Left*, and the ventral side to the *Bottom*. (*B*) In vivo whole-cell recording from a calyx (*Left*); upon constant-current injections (*Top*), the terminal showed a depolarizing sag, strong outward rectification, and a single AP (*Bottom*). Blue trace indicates the current threshold for eliciting an AP. Series resistance was compensated off-line. (*C*) In some recordings, evoked and spontaneous APs were followed by a postspike (arrow head), indicating a postsynaptic AP analogous to the prespike that can be recorded in postsynaptic recordings (24). (*D*) In voltage-clamp recordings, periods of spontaneous activity could be recorded (*Top*), which were composed of minibursts (*Bottom*). The ~2-Hz oscillation in the current amplitudes in the top recordings was induced by breathing. (*E*) Expansion of *D* illustrates two postspikes (arrowheads), and a lack of synaptic currents. For *D* and *E*, command potential was −80 mV; series resistance (36 MΩ) remained uncompensated.

In the first neonatal days, the terminal assumes a cup shape (18, 19, 27). Accompanying this structural development, a number of developmental changes in its biophysical properties occur (28, 29), including a developmental decrease in resting membrane resistance and a substantial increase in the outward rectification, a developmental trend for an increase in the maximal rate of rise, an increase in the rate of repolarization, and a clear shortening of the AP half-width (Fig. S1). APs elicited by brief current injections showed similar developmental changes. These developmental changes accelerated the terminal's AP, allowing firing at shorter intervals. Surprisingly, even P2–P3 calyces fired spontaneously over 150 Hz without apparent failures ($n = 3$, 4 calyces in whole-cell, juxtacellular mode, respectively), indicating that its ability to fire at high frequencies is already present shortly after its formation.

Resistance to Depression in Vivo. During high-frequency firing, the shape of the presynaptic AP remained remarkably constant in both whole-cell and juxtacellular recordings (Fig. 2 *A* and *B*). Fig. 2*C* shows the maximal rate of rise of the AP as a function of the inter-AP interval in a representative whole-cell recording. Whereas the postsynaptic somatic AP typically depresses >40% at the shortest intervals in vivo (22, 26, 30), the calyceal AP depressed on average only 4% for intervals <5 ms in whole-cell recordings (0.96 ± 0.03; mean ± SEM; $n = 9$ calyces; Fig. 2 *C* and *D*). Similar values were obtained for juxtacellular recordings (0.977 ± 0.004; mean ± SEM; $n = 18$ calyces; Fig. 2*D*), suggesting that this finding was not a consequence of washout, nor the result of R_s-related capacitive filtering. Moreover, within a miniburst, the maximal rate of rise of the third AP was similar to the first AP (time interval: 21 ± 2 ms; ratio AP_3/AP_1: 1.02 ± 0.01; mean ± SEM; $n = 9$ calyces), showing remarkable stability considering the high firing frequencies and the young age of the animals. In addition, following high-frequency bursting, the half-width, defined as the AP width at −35 mV, increased by only 4 ± 1% (mean ± SEM; $n = 9$; Fig. 2*D* and Fig. S3). In juxtacellular recordings, the AP half-width is best represented by the delay between the positive and negative peak (see figure 3*F* in ref. 30), and, similarly, in juxtacellular mode this delay increased by 4.0 ± 0.7% (mean ± SEM; $n = 18$; Fig. 2*D*). The change in half-width correlated with the AP depression ($r = -0.55$; $n = 27$; Fig. S3). We conclude that the shape of the presynaptic AP hardly changed during high-frequency activity.

We next investigated which mechanisms were responsible for the remarkable stability of the presynaptic AP shape. At short intervals, the membrane potential following the AP, V_{after}, will determine the onset potential of the next AP. To see how V_{after} affected the rate of rise of the next AP, we compared consecutive AP pairs during long depolarizing or hyperpolarizing current injections. Interestingly, if the calyceal membrane potential was hyperpolarized, the second AP would start at a more depolarized potential than the first and be relatively depressed; conversely, if the first AP started at a depolarized potential, the second AP would start at a more hyperpolarized potential and be potentiated compared with the first AP (Fig. 2*E*). To find the potential at which the depression reversed to potentiation, the relative change in the rate of rise of the second AP was plotted against the onset potential of the first AP (Fig. 2*F*). The potential at which the AP size was stable was obtained by linear regression. This stability potential V_{stab} was close to the resting membrane potential (RMP) (Fig. 2*G*), indicating that when V_{after} is close to the RMP, the AP shows minimal change in its rate of rise during high-frequency firing. We could not determine a V_{stab} for the AP half-width, as the half-width modulation did not change linearly with the onset potential, possibly due to inactivation of other voltage-dependent ion channels. Nevertheless, the half-width modulation fell within a limited range (0.95–1.05). We therefore conclude from our in vivo measurements that, if the membrane potential between APs is close to the RMP, the AP waveform remains stable during high-frequency firing.

In slice studies, the calyceal AP is typically followed by a 3- to 12-mV DAP (3, 15), yet in vivo we observed in 7 out of 17 recordings a HAP (Fig. 3*A*, *Inset*). The afterpotential did not change during development ($r = -0.1$; $n = 17$ calyces); it did depend on the RMP, with the direction of the afterpotential reversing at −71.3 ± 0.8 mV ($r = -0.88$; $n = 17$ calyces; Fig. 3*A*). To analyze how V_{after} changes when the AP started at different membrane potentials, we again looked at the long constant-current injections. V_{after}, measured 1.8 ms after the AP peak, seemed to be largely independent of the onset potential of the

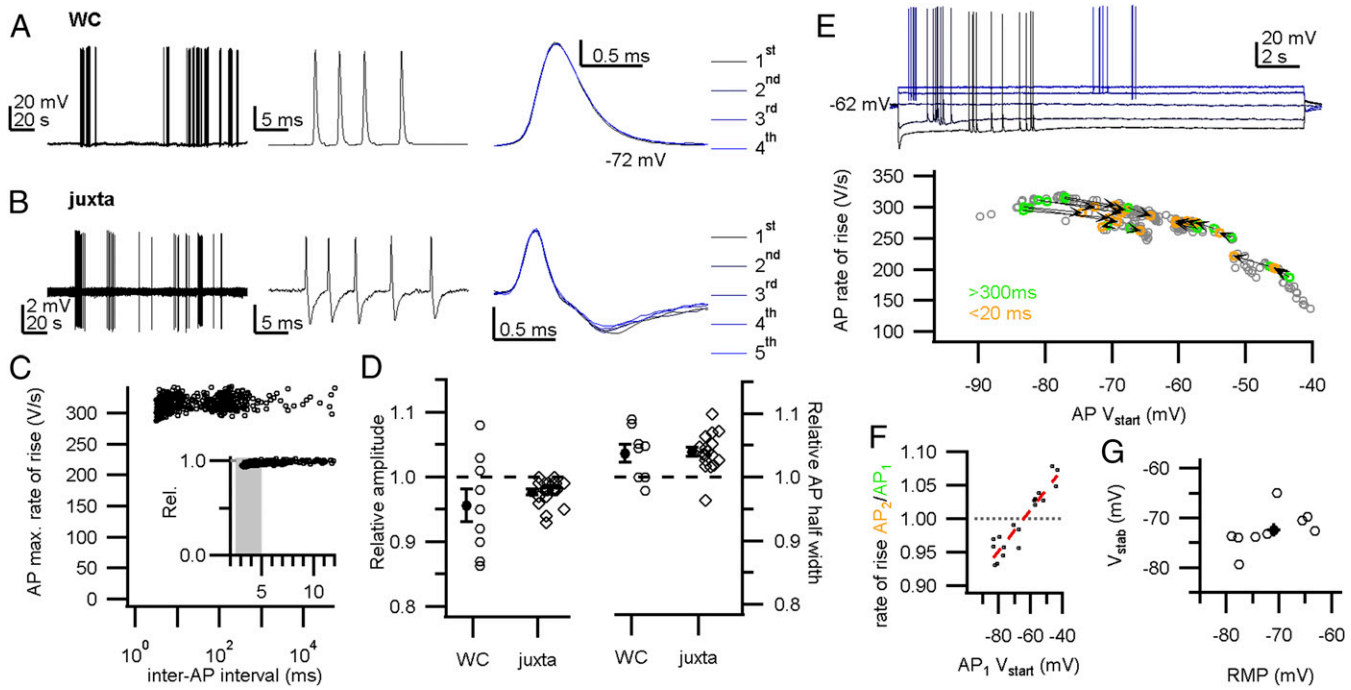

Fig. 2. Little AP depression during in vivo firing. (*A*, *Left*) In vivo whole-cell recording (WC) shows periods of calyceal bursting activity. (*Middle*) High-frequency miniburst. (*Right*) Overlay of the four APs. (*B*) In vivo juxtacellular recording (juxta) shows similar activity as in *A*, and an overlay of the five extracellular APs (eAPs) is shown (*Right*). (*C*) The maximal rate of rise against the inter-AP interval from a single whole-cell recording. (*Inset*) The maximal rate of rise relative to the preceding AP against the inter-AP interval shows a small but clear depression at short intervals. An average was calculated for the intervals within the gray area to compare between recordings. (*D*, *Left*) The relative amplitude at intervals below 5 ms shows a small depression. For WC, the relative change in AP rate of rise is shown; for juxta, the relative change in eAP amplitude. (*Right*) Changes in AP half-width for intervals <5 ms. (*E*, *Top*) Twenty seconds of constant-current injection with spontaneous burst firing. Constant-current injection started at −120 pA (lowest trace), incrementing 60 pA (indicated in blue shades). (*Bottom*) AP maximal rate of rise against the onset potential. Orange–green connected circle pairs correspond to a pair of APs of which the first AP (AP_1) was not preceded by an AP within 300 ms (green) and the second AP (AP_2) followed AP_1 within 20 ms (orange). (*F*) The relative rate of rise of the second AP in *E* against the onset potential of AP_1. Red broken line shows linear fit. Intersection with the black broken line where AP_2/AP_1 equals 1 was at −64.9 mV. (*G*) The stability potential (V_{stab}) vs. the resting membrane potential (RMP). The linear correlation was not significant [$r = 0.5$; $F_{(1,7)} = 2.8$; $P = 0.14$]. Circles in *C* and *E* indicate APs. Open markers in *D* and *G* indicate recorded calyces; closed markers correspond to averages. Circles in *F* indicate AP pairs. Bars indicate SEM.

AP in all recordings in which the AP started from −75 mV or more negative potentials (Fig. 3*A*), whereas at potentials more positive than −70 mV, V_{after} depolarized with a +0.58 ± 0.03 mV per mV change in the AP onset potential (mean ± SEM; n = 5 calyces; Fig. S4). Instead of focusing on the difference between the membrane potential before and after the AP (3, 15), we will focus on the absolute value of the membrane potential after the AP (V_{after}), which is more important for the impact on the next AP.

During burst activity, V_{after} becomes the onset potential of the next AP, which may thus keep onset potentials during a burst stable (7). Indeed, at high firing frequencies, the onset potential of an AP overlapped with V_{after} of its predecessor (Fig. 3*B*), and when the afterpotential was hyperpolarizing, the next AP could be potentiated (Fig. 3*B*). Furthermore, V_{after} was close to V_{stab} (Fig. 3*C*). During a period of increased activity, V_{after} became more depolarized, and the afterpotential could switch from hyperpolarizing to depolarizing (Fig. S4). On average, the afterpotential depolarized with 1.7 ± 0.2 mV during an active period [mean ± SEM; n = 9 calyces; paired t test AP_1 vs. AP_{15}: $t_{(8)} = 8.5$, $P < 0.01$], and although this change was statistically significant, such a small depolarization of the onset potential would only minimally change the AP properties (Fig. 2*E*). Considering the small size of the changes in the afterpotential during an active period, we conclude that V_{after} provides a stable AP onset potential at a value that keeps the AP waveform invariant.

Resistance to Depression in Slices. Two limitations of our in vivo recordings were the low-pass filtering related to the high series resistance and the inability to systematically test different afferent activity patterns. We therefore also made calyceal recordings in acute brainstem slices. Afferent fibers were stimulated via a bipolar stimulation electrode placed at the midline. With this approach, we tested whether depression would be more extensive at frequencies exceeding the frequencies observed in vivo (>400 Hz). At physiological temperatures, the calyx was able to fire at these frequencies (31), and the AP rate of rise depressed to 0.88 ± 0.02 at 2- to 3-ms intervals (mean ± SEM; n = 17; age, P4–P9). In 16 out of 17 terminals, we could determine both V_{stab} (−70 ± 1 mV; mean ± SEM) and V_{after} (−71 ± 1 mV; mean ± SEM). The two were again matched closely (r = 0.9; Fig. S5). V_{after} did not change in 2 mM calcium [n = 6; $\Delta V = 0.3 \pm 0.8$, $t_{(5)} = 0.9$, $P = 0.8$; Fig. S6], suggesting a limited role for calcium channels or calcium-activated channels in setting V_{after} (32). In addition, no effect of XE991 (10 μM) on the afterpotential was found [n = 5; $\Delta V = -0.6 \pm 0.7$, $t_{(5)} = 0.1$, $P = 0.5$; Fig. S6], suggesting that K_v7 channels did not significantly contribute to the first milliseconds of the afterpotential (32). Last, we quantified the stability of the AP shape during AP trains with different inter-AP intervals (2–100 ms). The waveform of the first AP differed from the other APs in the train (Fig. S7). The first AP was sensitive to the current injections (r = –0.95), whereas the second to fifth AP did not change (range of r = –0.4–0.2; Fig. S7), again indicating that the afterpotential stabilizes the calyceal AP shape.

During burst activity, the afterpotential affects AP depression by the time dependency of recovery from inactivation and the steady-state channel availability for the next AP. To disentangle

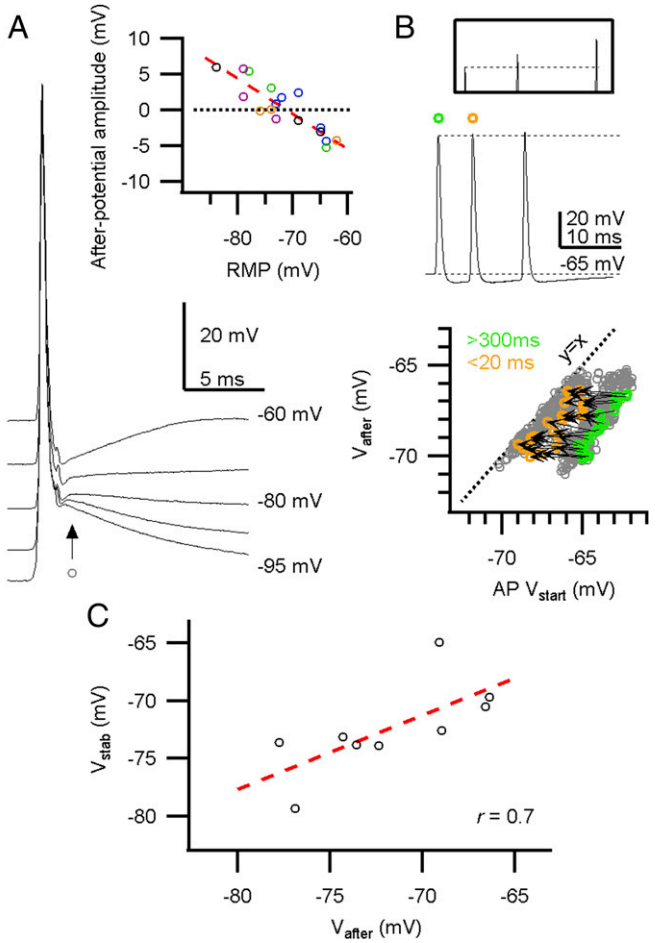

Fig. 3. During in vivo high-frequency firing, the membrane potential between APs is close to the potential at which APs are stable. (*A*) Five spontaneous, peak-aligned APs with different onset potentials due to constant-current injection. The afterpotential was measured at 1.8 ms (arrow) after the AP peak. (*Inset*) The afterpotential amplitude against the resting membrane potential (RMP). Circle color indicates pup age; black, blue, green, magenta, and orange are <P4, P4, P5, P6, >P6, respectively. (*B*, *Top*) A high-frequency burst with a HAP, and a potentiated AP amplitude (*Inset*). (*Bottom*) V_{after} against the onset potential (V_{start}). Gray circle is an AP; green–orange paired circles correspond to a pair of consecutive APs of which the first AP was not preceded by an AP within 300 ms (green), which was followed by a second AP within 20 ms (orange). The arrow represents the change in V_{after}–V_{start} for each pair. (*C*) The stability potential V_{stab} against the afterpotential V_{after}. Broken line depicts linear fit [$r = 0.7$; $F_{(1,7)} = 6.6$; $P = 0.04$]. The correlation suggests that V_{after} and V_{stab} are matched. For *A* and *C*, each circle corresponds to a different calyx.

the two effects, we modeled the AP depression (*SI Materials and Methods*). First, we measured the steady-state depression as a function of the onset potentials by means of current injections. These recordings indicated that the AP is slightly depressed at RMP (V_{half}: −54.8 ± 2.6 mV; k: 7.0 ± 0.9 mV; n = 14; mean ± SEM). Then, we used the steady-state depression to predict the depression induced by a stimulation train that was composed of multiple intervals representing in vivo-like activity with additional 2- to 3-ms intervals (Fig. S8*A*). The steady-state values did not capture the depression at the shortest intervals (one free parameter, explained variance: 60 ± 5%; n = 14; mean ± SEM; Fig. S8*C*). Adding recovery from depression, which included a voltage-dependent time constant as described in ref. 33, improved the prediction (two free parameters, explained variance: 86 ± 2%; n = 14; mean ± SEM; Fig. S8*D*), suggesting that steady-state recovery was not attained at the briefest interspike intervals. To reach 96% and 98% recovery from depression to the steady state associated with the onset potential of the next AP took 2.8 ± 0.2 and 3.5 ± 0.2 ms, respectively (mean ± SEM; n = 14; Fig. S8*B*), indicating that the intervals observed in vivo are sufficiently long for recovery to reach a steady state. Last, we tested to what extent the model with the average values could predict the depression in vivo by using the intervals and onset potentials observed in each experiment. The predicted depression matched the observed depression well for animals >P4 (n = 6; r = 0.9), whereas for P3–P4 the model underestimated the in vivo depression (−0.16 ± 0.2; n = 3; mean ± SEM; Fig. S8*E*). Together, these findings indicate that at P5 the rapid recovery from depression allows the calyx to fire at high frequencies with little or no AP depression.

Presence of $Na_v1.6$ in Calyx Terminals. The ability of the neonatal calyx of Held to fire at high frequencies with little depression suggests that it expresses sodium channel 1.6 ($Na_v1.6$) already shortly after its formation (23, 33). Brainstem sections of different postnatal ages were immunolabeled with a $Na_v1.6$ antibody. Already at P2–P3, weak expression was observed throughout the ventral auditory brainstem. The immunolabeling showed overlap with labeling for the vesicular glutamate transporter 1/2, but not with Ankyrin G (Fig. 4). No evidence for the presence of heminodes was obtained at this developmental stage. To confirm the presynaptic presence of $Na_v1.6$, we electroporated in vivo the calyceal axons with a fluorescent dye to label the axon that gives rise to the terminal, and again stained those terminals for $Na_v1.6$ and Ankyrin G. $Na_v1.6$ signal colocalized with the electroporated axons; no heminodes were observed (Fig. S9). Surprisingly, $Na_v1.6$ intensity was highest in the terminal itself (Fig. S9*B*), in contrast to a previous report (33), which might be related to the early developmental stage, at which no heminode has yet been formed (34, 35). We conclude that $Na_v1.6$ is already present at the calyx of Held shortly after its formation.

Discussion

Here, we report on in vivo whole-cell and juxtacellular recordings from the calyx of Held, a terminal whose accessibility for slice recordings has made it a popular subject for studying the

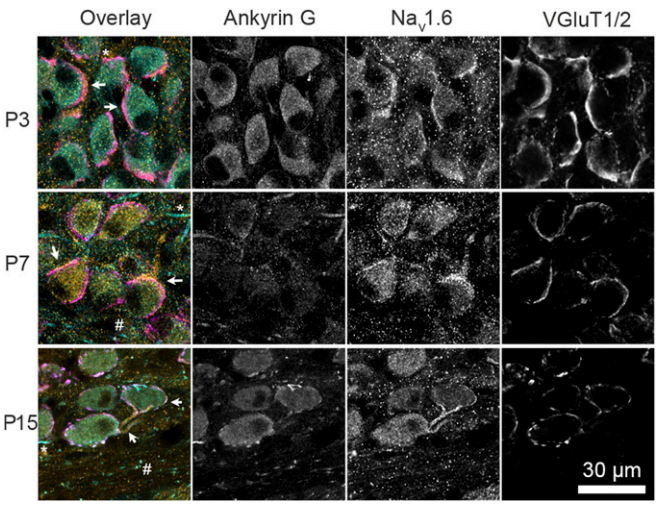

Fig. 4. Presynaptic immunolabeling of sodium channel 1.6 during postnatal development. Confocal images of the MNTB (P3, P7, and P15 rat) that were immunolabeled for Ankyrin G, sodium channel 1.6 ($Na_v1.6$), and vesicular glutamate transporter 1/2 (VGluT1/2) reveal colocalization of the strongest $Na_v1.6$ labeling with presynaptic VGluT1/2 (arrows). The Ankyrin G antibody marks axon initial segments (*), nodes of Ranvier (#), and heminodes. Conclusive distinction between heminodes and nodes of Ranvier was not possible based on this panel of antibodies.

biophysics of transmitter release. In developing rodents, the calyx of Held fired in a burst manner at >200 Hz with no sign of failures, remarkably little depression or broadening of the AP, and rapid recovery from AP depression. We defined the stability potential, V_{stab}, as the membrane potential following the AP at which the next AP would not change shape, and found it to be close to the RMP. Moreover, the membrane potential following the AP (V_{after}) was close to V_{stab}, which means that during high-frequency firing, when V_{after} determined the onset potential of the next AP, AP stability was maximized. Immunolabeling indicated that the sodium channel $Na_v1.6$ was already present in newly formed calyces, providing a molecular basis for the observed lack of AP depression both in slices and in vivo. These results thus demonstrate important mechanisms underlying fast signaling during natural firing of the calyx of Held.

Mechanisms Limiting AP Depression During Natural Activity. We observed that the shape of the calyceal AP was remarkably invariant during in vivo firing. Even though instantaneous firing frequencies of 200 Hz were observed already at P2–P3 when the calyx forms, there was little AP depression. Two factors appeared to be crucially important for the lack of a change in the AP's shape: fast recovery from AP depression and a membrane potential between APs that minimized waveform changes.

The AP depression obtained in slice recordings was largely independent from the interval between APs. Only at the 2- to 4-ms intervals was a time-dependent component in the recovery observed. The combination of a steady-state depression with a time-dependent recovery adequately described the observed AP depression, suggesting that the fast recovery of calyceal sodium channels from inactivation (33) provided a reasonable description of the recovery from AP depression. Immunolabeling evidence was obtained for the early presence of $Na_v1.6$, which is known for its swift kinetics and resistance to inactivation during high-frequency firing (36); the presence of $Na_v1.6$ is in agreement with studies at the calyx of Held at later developmental stages (33, 34, 35). No evidence was found for the presence of heminodes, which do not form until the second postnatal week, presumably triggered by myelination (15, 34, 35, 37). An increase in glial coverage and the replacement of the cup shape by the calyceal fingers precluded an investigation of the properties of the mature calyx in vivo. The mature calyx has even briefer APs after hearing onset (28), to which an exclusion of sodium channels from the calyx may contribute (33).

A second contributing factor to the resistance to spike depression in vivo was that V_{after} was close to V_{stab}, the potential at which the shape of the AP became invariant. The in vivo RMP, which was also close to V_{after}, was within the same range as previous slice reports, although in most cases a more negative RMP and a larger DAP were reported (3, 24, 28, 38–40). Assuming that the larger DAP is due to the more negative RMP, a difference in temperature might explain the difference with many of the earlier slice experiments, because the RMP of the calyx tends to be more depolarized at physiological temperatures (41), and many of the earlier slice experiments were done at room temperature. As the RMP at the calyx of Held is set by the potassium channel subunit $K_v7.5$ (38), I_h (42), the Na^+/K^+-ATPase (43), and a persistent sodium channel (39), subtle differences in any of these four conductances (or driving forces) may be responsible for the observed small difference in RMP compared with some previous slice studies. Apart from $K_v7.5$, for which blocking showed little effect on V_{after}, these conductances are also likely to contribute to setting V_{after}, with an additional prominent role for K_v1 channels (40, 44) and resurgent sodium channels (15).

Resurgent sodium currents not only make an important contribution to the afterpotential of the calyx of Held, they also promote faster APs and higher frequency signaling (15). Most likely, the resurgent sodium currents reflect the unblocking of a pore-blocking particle from the auxiliary $Na_v\beta4$ channel subunit, which can rapidly block $Na_v1.6$ upon opening (23). The blocking particle allows for brief APs, and it limits sodium channel inactivation. At very short intervals, facilitation of K channels may also contribute to keeping the APs brief (45). Rapid closure of axonal sodium channels is expected to increase the energetic efficiency of the AP (46). The transient opening of the sodium channel due to the unblocking of this particle at negative potentials has been viewed as a by-product, but we suggest that the resurgent current serves to set V_{after} close to V_{stab}, thereby sustaining invariant AP firing. Together, these adaptations thus allow remarkably stable APs, even at high firing frequencies.

Functional Implications. In general, the afterpotential controls the availability of voltage-dependent ion channels during high-frequency signaling and sets the onset potential of the next AP. More specific functions have been proposed for the afterpotential in terminals. The DAP may be responsible for increased excitability following an AP in hippocampal Schaffer collaterals (47), but a large DAP may lead to sodium channel inactivation and spike failures (15). A decrease in presynaptic AP amplitude might contribute to short-term depression (1), although these changes might be counteracted by a broadening of the AP (48). By controlling the deactivation of Ca^{2+} channels, the afterpotential may directly control transmitter release, but a recent study at the calyx of Held found the total calcium influx to be largely independent of the value of the afterpotential (49). At hippocampal mossy fiber terminals, the DAP may contribute to cumulative inactivation of K_v1 channels, resulting in spike broadening (5), and thereby contributing to the strong synaptic facilitation during high-frequency bursts (5, 50). The transmission characteristics of this synapse differ substantially from the relay function of the calyx of Held synapse (16) or the cerebellar mossy fiber synapse (4), and this difference might partially be a consequence of V_{after} being more depolarized than V_{stab}. For en passant boutons, the impedance mismatch imposed by their geometrical shape makes the axon vulnerable for frequency-dependent propagation failures (1). The use of voltage indicators (7, 12, 13) might allow testing of whether the mechanisms identified here may also help to stabilize AP speed and secure AP propagation in boutons.

We propose that, in agreement with data obtained in the crayfish neuromuscular junction (7), an important function of the afterpotential is to preserve the shape of the presynaptic AP. The close correspondence of RMP, V_{stab}, and V_{after} makes not only the onset potential of AP remarkably independent of firing frequency, but also results in a remarkably stable AP shape. For a relay synapse such as the calyx of Held, which excels in being precise and reliable over a wide range of firing frequencies (16), this has obvious advantages. Changes in AP shape due to a change in sodium channel availability will not only affect the opening of calcium channels, the timing and amplitude of Ca^{2+}-influx, and neurotransmitter release, but will also affect axonal propagation speed, resulting in a loss of timing precision (2). We conclude that our in vivo recordings of the calyx of Held provide insights into the mechanisms that keep APs stable. Future experiments may clarify how the relation between V_{after} and V_{stab} is controlled, and whether their relation can be dynamically adjusted at the calyx of Held and other presynaptic terminals.

Materials and Methods

All experiments complied with institutional and European guidelines, and were approved by the animal ethical committee of the Erasmus MC. Briefly, timed-pregnancy Wistar dams were purchased from Envigo or Charles River and were housed within the animal facility of the Erasmus MC. The day of birth was taken as P0. Neonate pups were anesthetized with isoflurane, intubated, and mechanically ventilated, and underwent a ventral approach to expose the right ventral brainstem (22, 51). Before the recordings, anesthesia was reduced to 1% isoflurane, which kept the animal areflexive. The in vivo electroporation with Alexa Fluor 594–dextran (Molecular Probes) was described in ref. 51. The in vivo electrophysiological methods are detailed in ref. 22. Junction potential of the K-gluconate–based intrapipette solution (−11 mV) was corrected. Gigaseal formation was obtained by gentle suction followed by pipette capacitance (C_p) compensation in voltage-clamp mode

of the Axopatch 200B (Molecular Devices). Brief suction was applied to establish the whole-cell configuration, and the RMP was measured immediately after break-in. Voltage recordings were made in CC-fast mode. The recordings were low-pass filtered (four-pole Bessel; 10 kHz) and digitized at 25 kHz. Series resistances (R_s) were measured (Fig. S1), but the voltage drop across R_s was corrected off-line.

Acute brainstem slices were made as reported in ref. 3. R_s was fully compensated. C_p was compensated either in voltage-clamp or in current-clamp mode. Recordings were low-pass filtered (four-pole Bessel; 10 kHz) and digitized at 25 or 50 kHz. Custom-written analyses were made in the Igor Pro environment (Wavemetrics). For the depression model, we only included the recordings for which >70% of the total variance was explained (n = 14 of 17).

The biocytin fluorescent labeling procedure has been described elsewhere (22). For the immunolabeling of sodium channel 1.6, brainstem sections (40 μm) underwent antigen retrieval by 3-h incubation at 80 °C in 10 mM sodium citrate; they subsequently followed the same immunolabeling procedure as detailed in refs. 22 and 52 with Tris-buffered solutions (pH 7.6). More details can be found in *SI Materials and Methods*.

ACKNOWLEDGMENTS. We thank Kees Donkersloot for technical support, Elize Haasdijk and Erika Goedknegt for support with histology, Fereshta Zakeri for performing control immunolabelings, and Maarten Kole for helpful comments. The confocal scanning microscope was accessed through the Optical Imaging Center at Erasmus MC. The research was funded by the Nederlandse Organisatie voor Wetenschappelijk Onderzoek–Aard- en Levenswetenschappen ("Development of a Giant Synapse"; 823.02006).

1. Debanne D, Campanac E, Bialowas A, Carlier E, Alcaraz G (2011) Axon physiology. *Physiol Rev* 91:555–602.
2. Bucher D, Goaillard JM (2011) Beyond faithful conduction: Short-term dynamics, neuromodulation, and long-term regulation of spike propagation in the axon. *Prog Neurobiol* 94:307–346.
3. Borst JGG, Helmchen F, Sakmann B (1995) Pre- and postsynaptic whole-cell recordings in the medial nucleus of the trapezoid body of the rat. *J Physiol* 489:825–840.
4. Rancz EA, et al. (2007) High-fidelity transmission of sensory information by single cerebellar mossy fibre boutons. *Nature* 450:1245–1248.
5. Geiger JR, Jonas P (2000) Dynamic control of presynaptic Ca^{2+} inflow by fast-inactivating K^+ channels in hippocampal mossy fiber boutons. *Neuron* 28:927–939.
6. Barrett EF, Barrett JN (1982) Intracellular recording from vertebrate myelinated axons: Mechanism of the depolarizing afterpotential. *J Physiol* 323:117–144.
7. Lin JW (2008) Electrophysiological events recorded at presynaptic terminals of the crayfish neuromuscular junction with a voltage indicator. *J Physiol* 586:4935–4950.
8. Powell K, Mathy A, Duguid I, Häusser M (2015) Synaptic representation of locomotion in single cerebellar granule cells. *eLife* 4:4.
9. Begum R, Bakiri Y, Volynski KE, Kullmann DM (2016) Action potential broadening in a presynaptic channelopathy. *Nat Commun* 7:12102.
10. Llinás R, Steinberg IZ, Walton K (1981) Presynaptic calcium currents in squid giant synapse. *Biophys J* 33:289–321.
11. Poage RE, Zengel JE (2002) Repolarization of the presynaptic action potential and short-term synaptic plasticity in the chick ciliary ganglion. *Synapse* 46:189–198.
12. Hoppa MB, Gouzer G, Armbruster M, Ryan TA (2014) Control and plasticity of the presynaptic action potential waveform at small CNS nerve terminals. *Neuron* 84: 778–789.
13. Ford KJ, Davis GW (2014) Archaerhodopsin voltage imaging: Synaptic calcium and BK channels stabilize action potential repolarization at the *Drosophila* neuromuscular junction. *J Neurosci* 34:14517–14525.
14. Hu H, Jonas P (2014) A supercritical density of Na^+ channels ensures fast signaling in GABAergic interneuron axons. *Nat Neurosci* 17:686–693.
15. Kim JH, Kushmerick C, von Gersdorff H (2010) Presynaptic resurgent Na^+ currents sculpt the action potential waveform and increase firing reliability at a CNS nerve terminal. *J Neurosci* 30:15479–15490.
16. Borst JGG, Soria van Hoeve J (2012) The calyx of Held synapse: From model synapse to auditory relay. *Annu Rev Physiol* 74:199–224.
17. Guinan JJ, Jr, Li RY-S (1990) Signal processing in brainstem auditory neurons which receive giant endings (calyces of Held) in the medial nucleus of the trapezoid body of the cat. *Hear Res* 49:321–334.
18. Kandler K, Friauf E (1993) Pre- and postnatal development of efferent connections of the cochlear nucleus in the rat. *J Comp Neurol* 328:161–184.
19. Hoffpauir BK, Grimes JL, Mathers PH, Spirou GA (2006) Synaptogenesis of the calyx of Held: Rapid onset of function and one-to-one morphological innervation. *J Neurosci* 26:5511–5523.
20. Rodríguez-Contreras A, de Lange RPJ, Lucassen PJ, Borst JGG (2006) Branching of calyceal afferents during postnatal development in the rat auditory brainstem. *J Comp Neurol* 496:214–228.
21. Wang HC, Bergles DE (2015) Spontaneous activity in the developing auditory system. *Cell Tissue Res* 361:65–75.
22. Sierksma MC, Tedja MS, Borst JGG (2017) In vivo matching of postsynaptic excitability with spontaneous synaptic inputs during formation of the rat calyx of Held synapse. *J Physiol* 595:207–231.
23. Lewis AH, Raman IM (2014) Resurgent current of voltage-gated Na^+ channels. *J Physiol* 592:4825–4838.
24. Forsythe ID (1994) Direct patch recording from identified presynaptic terminals mediating glutamatergic EPSCs in the rat CNS, in vitro. *J Physiol* 479:381–387.
25. Tritsch NX, et al. (2010) Calcium action potentials in hair cells pattern auditory neuron activity before hearing onset. *Nat Neurosci* 13:1050–1052.
26. Crins TTH, Rusu SI, Rodríguez-Contreras A, Borst JGG (2011) Developmental changes in short-term plasticity at the rat calyx of Held synapse. *J Neurosci* 31:11706–11717.
27. Morest DK (1968) The growth of synaptic endings in the mammalian brain: A study of the calyces of the trapezoid body. *Z Anat Entwicklungsgesch* 127:201–220.
28. Taschenberger H, von Gersdorff H (2000) Fine-tuning an auditory synapse for speed and fidelity: Developmental changes in presynaptic waveform, EPSC kinetics, and synaptic plasticity. *J Neurosci* 20:9162–9173.
29. Chuhma N, Ohmori H (1998) Postnatal development of phase-locked high-fidelity synaptic transmission in the medial nucleus of the trapezoid body of the rat. *J Neurosci* 18:512–520.
30. Lorteije JAM, Rusu SI, Kushmerick C, Borst JGG (2009) Reliability and precision of the mouse calyx of Held synapse. *J Neurosci* 29:13770–13784.
31. Taschenberger H, Leão RM, Rowland KC, Spirou GA, von Gersdorff H (2002) Optimizing synaptic architecture and efficiency for high-frequency transmission. *Neuron* 36:1127–1143.
32. Bean BP (2007) The action potential in mammalian central neurons. *Nat Rev Neurosci* 8:451–465.
33. Leão RM, et al. (2005) Presynaptic Na^+ channels: Locus, development, and recovery from inactivation at a high-fidelity synapse. *J Neurosci* 25:3724–3738.
34. Berret E, Kim SE, Lee SY, Kushmerick C, Kim JH (2016) Functional and structural properties of ion channels at the nerve terminal depends on compact myelin. *J Physiol* 594:5593–5609.
35. Xu J, Berret E, Kim JH (2017) Activity-dependent formation and location of voltage-gated sodium channel clusters at a CNS nerve terminal during postnatal development. *J Neurophysiol* 117:582–593.
36. Zhou W, Goldin AL (2004) Use-dependent potentiation of the $Na_v1.6$ sodium channel. *Biophys J* 87:3862–3872.
37. Kaplan MR, et al. (2001) Differential control of clustering of the sodium channels $Na_v1.2$ and $Na_v1.6$ at developing CNS nodes of Ranvier. *Neuron* 30:105–119.
38. Huang H, Trussell LO (2011) KCNQ5 channels control resting properties and release probability of a synapse. *Nat Neurosci* 14:840–847.
39. Huang H, Trussell LO (2008) Control of presynaptic function by a persistent Na^+ current. *Neuron* 60:975–979.
40. Ishikawa T, et al. (2003) Distinct roles of Kv1 and Kv3 potassium channels at the calyx of Held presynaptic terminal. *J Neurosci* 23:10445–10453.
41. Kim JH, von Gersdorff H (2012) Suppression of spikes during posttetanic hyperpolarization in auditory neurons: The role of temperature, I_h currents, and the Na^+-K^+-ATPase pump. *J Neurophysiol* 108:1924–1932.
42. Cuttle MF, Rusznák Z, Wong AY, Owens S, Forsythe ID (2001) Modulation of a presynaptic hyperpolarization-activated cationic current (I_h) at an excitatory synaptic terminal in the rat auditory brainstem. *J Physiol* 534:733–744.
43. Kim JH, Sizov I, Dobretsov M, von Gersdorff H (2007) Presynaptic Ca^{2+} buffers control the strength of a fast post-tetanic hyperpolarization mediated by the α3 Na^+/K^+-ATPase. *Nat Neurosci* 10:196–205.
44. Dodson PD, et al. (2003) Presynaptic rat Kv1.2 channels suppress synaptic terminal hyperexcitability following action potential invasion. *J Physiol* 550:27–33.
45. Yang YM, et al. (2014) Enhancing the fidelity of neurotransmission by activity-dependent facilitation of presynaptic potassium currents. *Nat Commun* 5:4564.
46. Alle H, Roth A, Geiger JRP (2009) Energy-efficient action potentials in hippocampal mossy fibers. *Science* 325:1405–1408.
47. Soleng AF, Baginskas A, Andersen P, Raastad M (2004) Activity-dependent excitability changes in hippocampal CA3 cell Schaffer axons. *J Physiol* 560:491–503.
48. Borst JGG, Sakmann B (1999) Effect of changes in action potential shape on calcium currents and transmitter release in a calyx-type synapse of the rat auditory brainstem. *Philos Trans R Soc Lond B Biol Sci* 354:347–355.
49. Clarke SG, Scarnati MS, Paradiso KG (2016) Neurotransmitter release can be stabilized by a mechanism that prevents voltage changes near the end of action potentials from affecting calcium currents. *J Neurosci* 36:11559–11572.
50. Bischofberger J, Engel D, Frotscher M, Jonas P (2006) Timing and efficacy of transmitter release at mossy fiber synapses in the hippocampal network. *Pflugers Arch* 453: 361–372.
51. Rodríguez-Contreras A, van Hoeve JS, Habets RLP, Locher H, Borst JGG (2008) Dynamic development of the calyx of Held synapse. *Proc Natl Acad Sci USA* 105: 5603–5608.
52. de Ruiter MM, De Zeeuw CI, Hansel C (2006) Voltage-gated sodium channels in cerebellar Purkinje cells of mormyrid fish. *J Neurophysiol* 96:378–390.
53. Jenkins SM, Bennett V (2001) Ankyrin-G coordinates assembly of the spectrin-based membrane skeleton, voltage-gated sodium channels, and L1 CAMs at Purkinje neuron initial segments. *J Cell Biol* 155:739–746.
54. Black JA, Renganathan M, Waxman SG (2002) Sodium channel $Na_v1.6$ is expressed along nonmyelinated axons and it contributes to conduction. *Brain Res Mol Brain Res* 105:19–28.